Multi-spatiotemporal AOD trends and association with land use changes over the Guangdong-Hong Kong-Macao Greater Bay Area during 2001-2021

Xinyu Yu [1], Man Sing Wong [1,2*], Chun-Ho Liu [3]

[1] Department of Land Surveying and Geo-Informatics, The Hong Kong Polytechnic University, Hung Hom, Hong Kong, China;

[2] Research Institute for Land and Space, The Hong Kong Polytechnic University, Hung Hom, Hong Kong, China

[3] Department of Mechanical Engineering, The University of Hong Kong, Pokfulam Road, Hong Kong, China

** Correspondence: Ls.charles@polyu.edu.hk Tel: +852 3400 8959*

Abstract

Analyzing long-term variations of aerosol optical depth (AOD) is beneficial for determining high-pollutant-risk areas and formulating mitigation policies. In this study, multi-spatiotemporal trends and periodicity of AOD, as well as the persistence over the Guangdong-Hong Kong-Macao Greater Bay Area from 2001 to 2021 were investigated by the extreme-point symmetric mode decomposition (ESMD), Theil-Sen Median trend analysis, and Hurst exponent. The results elucidate that AOD exhibits fluctuant variations during the 21-year period with the year 2012 as the turning point. There is a slight upward tendency (0.009 yr^{-1}) in the pre-2012 period but a pronounced downward trend (-0.03 yr^{-1}) in the post-2012 period, suggesting an overall declining trend in the study area. The northern cities in the area present an increasing-stable-decreasing trend of monthly-average AOD, whereas other cities have an increasing-fluctuating-decreasing trend over the study period. The decreasing rate in the western parts is higher than that in the eastern parts, like Zhaoqing, Jiangmen and Foshan city. A continuous decline of AOD is dominated over the study area, whereas an anti-persistence tendency is accumulated in the northeastern parts. Additionally, elevated AOD can be observed in unused land, water bodies and construction land, while grassland, cropland and woodland have lower AOD. The decreasing rate is larger when land-use types with high AOD are converted to those with low AOD, otherwise, the decreasing rate is smaller. The results have a great significance for improving the understanding of long-term variations of AOD, as well as providing a scientific basis to formulate environmental protection and mitigation practices.

Keywords: Aerosol optical depth; multi-spatiotemporal trends; extreme-point symmetric mode decomposition; Theil-Sen Median trend analysis; Hurst exponent; land use changes.

1. Introduction

Aerosol is defined as liquid or solid particles suspended in the atmosphere with different size distributions and shapes, and originated from different sources, which plays a pivotal role in air quality and climate change (Wong et al., 2011; Wong et al., 2010; Kim et al., 2014). Aerosols have a significant impact on the Earth's radiance balance and climate change directly and indirectly, via its properties of absorbing and scattering solar radiation and aerosol-cloud interactions (Satheesh & Moorthy, 2005; Charlson et al., 1992; Ramanathan et al., 2001); as well as have impacts on the ecosystem and human health (Liu et al., 2017; Silva et al., 2013). AOD is a quantitative indicator to represent extinction characteristics of atmospheric aerosol and air pollution at a national and regional scale (Liu et al., 2004). Although emission control measures have been gradually implemented by the national and local governments, with the rapid urbanization and industrialization in China, air pollution issues and aerosol particles caused by increasing anthropogenic emissions have consequently become more prominent (Qin et al., 2016; Zhang et al., 2012). As increasing or decreasing aerosol loadings in the atmosphere can impinge on monsoon circulation, atmospheric and hydrological cycle, thereby resulting in regional and global climate changes (Wu et al., 2013; Che et al., 2019; Shu et al., 2022). Thus, investigating the long-term spatiotemporal variation trends of AOD at regional and finer scales is vital to strengthen the understanding of our climate and planning for future mitigation strategies.

Initially, AOD was monitored and observed based on Aerosol Robotic Network (AERONET) or other ground-based instruments, but the sparse and uneven spatial distribution of the ground-based measurements limits the representation of AOD spatiotemporal characteristics to a regional perspective (Wang et al., 2019). In contrast, satellite-based observations can compensate for and complement the deficiencies of ground-based measurements. Currently, various sensing platforms have been developed to cater to the demands of aerosol monitoring and analysis, including Advanced Himawari Imager (AHI), Moderate Resolution Imaging Spectroradiometer (MODIS), Multi-angle Imaging Spectroradiometer (MISR), Ozone Monitoring Instrument (OMI) and Cloud-Aerosol Lidar and Infrared Pathfinder Satellite Observation (CALIPSO) (Wong et al., 2013b). Among them, the MODIS aerosol product (MCD19A2) can provide daily global AOD with 1-km spatial resolution via the multi-angle inversion atmospheric correction (MAIAC) approach from February 2000. Moreover, its superior accuracy has been proclaimed by numerous researchers (Lyapustin et al., 2011; Superczynski et al., 2017). By virtue of the elevated spatiotemporal resolution of the MCD19A2 dataset, it has been widely used for various applications (Martins et al., 2019; Lu et al., 2021).

Intensive research about the spatiotemporal distributions and variations of AOD in China has been conducted in previous studies. For example, He et al. (2016) presented an upward trend from 2002 to 2007 and a downward trend from 2008 by analyzing the AOD trends in China from 2002 to 2015 using the MODIS 3-km AOD product. Sogacheva et al. (2018) adopted multi-satellite observations between 1995 and 2017 and found that there was an initial increase followed by a gradual decrease from 2011. Similarly, the AOD in the eastern and central China experienced an increase before 2006 caused by rapid economic development and a significant decrease from 2011 with slight variations between 2006 and 2011 (Zhao et al., 2017; Shu et al., 2022; He et al., 2020).

Among most of the previous studies, linear regression was widely used for trend analysis. Nevertheless, it is sensitive to outliers and struggles to provide the variations of AOD from a spatial perspective. It is more applicable on processing normally distributed data, while atmospheric parameters sometimes exhibit non-normally distributed patterns (Yin, 2021; Munir et al., 2013). In contrast, the extreme-point symmetric mode decomposition (ESMD) method, which is a newly developed statistical method, can be used to capture non-linear variation trends and periodic changes of time-series sequence regardless of the distribution patterns (Wang & Li, 2013). The ESMD approach has been used effectively to reveal non-linear and periodic trends of climate-related issues (Wang et al., 2020; Qin et al., 2018). Here, it was used to investigate the non-linear AOD tendency for different districts. Additionally, the Theil-Sen Median trend analysis was used to identify the varying trends for each grid quantitatively (Sen, 1968; Theil, 1950), which is insensitive to individual outliers and is capable of characterizing the changing trends of time-series sequence (Wang et al., 2022). It was widely adopted for analyzing the varying trends from the spatiotemporal perspective in temperature changes (Tabari et al., 2012), hydrological sequence data (Dinpashoh et al., 2011) and vegetation variation (Jiang et al., 2015). Furthermore, the sustainability of AOD trends was rarely involved and analyzed in previous studies, which can reveal the varying trend directions in the future and provide implications for corresponding policy regulations. For estimating the persistence and anti-persistence of time-series datasets, the Hurst exponent approach was frequently applied in drought evolution (Tong et al., 2018), hydrothermal climate changes (Ma et al., 2018) and $PM_{2.5}$ concentration changes (Wang et al., 2022). To the best of our knowledge, exploration and discussion of AOD tendency persistence based on the Hurst exponent have not yet been conducted.

A substantial research effort on aerosol variation analysis has been implemented, which has provided meaningful implications and promotion (Pozzer et al., 2015; Zhang et al., 2016; He et al., 2019). Most of the aforementioned studies have been conducted nationwide or in areas with severe air pollution, however, fewer analyses have been implemented in the Guangdong-Hong Kong-Macao Greater Bay Area (the GBA), resulting in distinct and specific characteristics of AOD distribution and long-term changing trends in the GBA being ignored. The GBA is one of the largest metropolitan regions in China, where has experienced accelerating urbanization and industrialization. Generally, urban expansion is commonly accompanied by remarkable land use/land cover change (LULCC, Deng et al., 2009). Previous studies have demonstrated that land use/land cover (LULC) types are highly associated with the distribution and changes of AOD (Li et al., 2018; Liu et al., 2020). However, the influence of LULCC on AOD variations lacks detailed analysis. Thus, further studies to quantify the influence of LULC types and LULCC on AOD changing trends over highly urbanized and industrialized regions are of vital scientific merits.

In this study, the AOD datasets from the MCD19A2 product were employed to analyze multi-spatiotemporal AOD trends and tendency persistence across the GBA from 2001 to 2021 based on the ESMD, Theil-Sen Median trend analysis, Mann-Kendall test and Hurst exponent approach. The major objectives can be summarized as follows: (1) to identify the spatiotemporal patterns and regional discrepancies of AOD variations during the 21-year period; (2) to untangle the trends and periodicity of AOD at multiple spatiotemporal scales, as well as its persistence to assist a

comprehensive understanding of AOD changes; (3) to investigate the impacts of LULCC on AOD variations, and the results can provide a scientific basis for policymakers to implement appropriate AOD mitigation measures.

2. Study area and data collection

2.1 Study area

The GBA composes of Hong Kong Special Administrative Region (SAR), Macao SAR, two megacities like Guangzhou and Shenzhen and seven medium-sized cities, including Dongguan, Foshan, Jiangmen, Huizhou, Zhaoqing, Zhongshan, and Zhuhai in Guangdong Province (Figure 1). It is one of the largest metropolitan regions in China with rapid economic and urbanization development. Understanding the long-term variations of AOD across the whole GBA region is critical to providing useful references for environmental protection policy formulation.

2.2 AOD datasets

MODIS provides retrieval AOD products based on different approaches, including MAIAC, Deep Blue (DB) and Dark Target (DT). Moreover, the MCD19A2 product (https://lpdaac.usgs.gov/products/mcd19a2v006/) can provide daily frequency and 1-km spatial resolution of aerosol products retrieved by MAIAC algorithm in global coverage with higher retrieval quality and accuracy (Xiao et al., 2017; Liu et al., 2019). In this paper, MCD19A2 AOD at 0.55 μm was used owing to the consistency and relatively stable quality (Lyapustin et al., 2018).

To alleviate the uncertainties and ensure the accuracy of the retrieved AOD, data pre-processing was instigated to maintain the consistency of AOD data. First, a data filter is supposed to be applied based on the quality assurance (QA) file. Specifically, in addition to the cloud-free AOD retrievals, the QA.CloudMask = Possibly_Cloudy was suggested to define high quality by assuming a certain degree of aerosol spatial homogeneity. Besides, pixels with the QA filter for AOD within $\pm$2 km from the coastline were included as majority urban built-up areas in the GBA are close to the coastline (Shi et al., 2021). Afterwards, daily, monthly and yearly averaged AOD were calculated based on valid retrievals.

2.3 Land use/land cover dataset

LULC datasets were acquired from the MODIS land use product (MCD12Q1) with yearly intervals and the spatial resolution of 500 m during 2001-2020 (https://lpdaac.usgs.gov/products/mcd12q1v006/). The MCD12Q1 dataset divides the LULC types into 17 classes according to the International Geosphere-Biosphere Programme classification scheme. In this study, we reclassified the LULC types into six categories, including woodland, grassland, construction land, cropland, water and unused land. Additionally, the LULC types were resampled to 1-km spatial resolution to maintain consistency with AOD data.

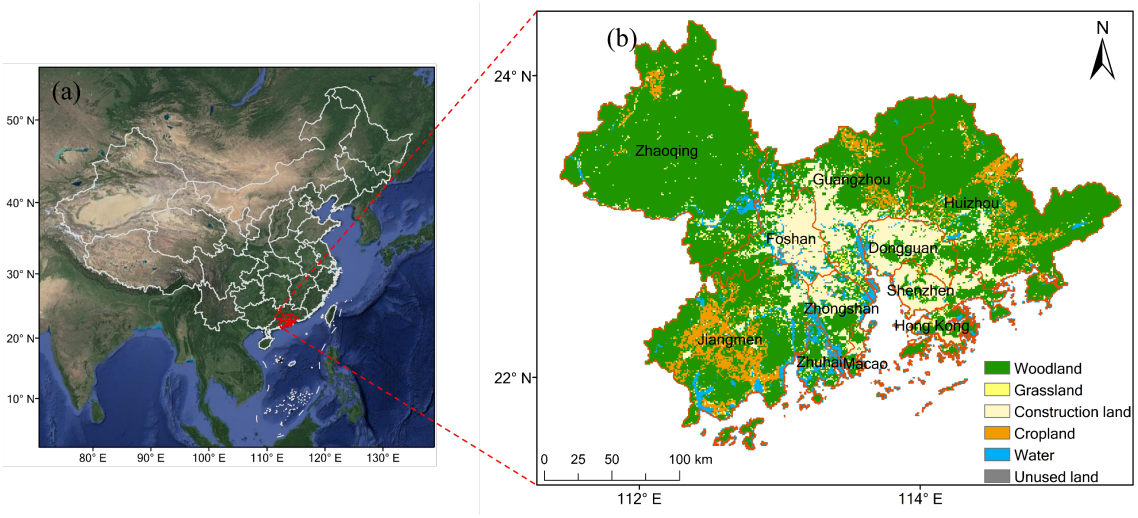

Figure 1. (a) Geographical location of the study area; (b) the background map displays the spatial distribution of LULC types in 2020 across the GBA region.

3. Methodology

3.1 Extreme-point symmetric mode decomposition (ESMD)

ESMD was proposed based on empirical mode decomposition (EMD, Wang & Li, 2013), which can be used to detect the time-dependent non-linear tendency without antecedent assumption. After using ESMD, original signals can be decomposed into several intrinsic mode functions (IMFs) and a residual curve (R). Generally, the IMFs contain periodic oscillations (i.e., annual and seasonal periodicity) and irregular non-periodic changes caused by unexpected factors, like weather conditions, short-term pollution control policies and human activity intensity (Zheng et al., 2022). The residual curve derived by ESMD is used to denote the de-seasonalized variation tendency. Compare to the monotonous variation trend, ESMD provide non-linear varying trends, which can reflect more detailed fluctuations.

$$Y(m) = \sum_{i=1}^{n} M_i(m) + R(m) \quad (1)$$

where $M_i(m)$ is the i^{th} IMF; $R(m)$ is the tendency curve and n denotes the total number of IMFs. Detailed decomposition process can be found in the supplementary materials. In our study, R denotes the monthly-scale AOD trend from 2001 to 2021.

3.2 Theil-Sen median trend analysis and the Mann-Kendall test

The Theil-Sen median trend analysis is a robust trend analysis method by calculating the median of slopes estimated between the paired datasets (Theil, 1950; Sen, 1968). It was widely applied for exploring the inter-annual changes as it is not interfered by outliers and generates reliable results (Wilcox, 2001). In our study, this approach was applied for the long-term spatiotemporal variation trend analysis of AOD in the study area. It can be expressed as follows:

$$\beta = Median\left(\frac{x_j - x_i}{j - i}\right),\ i < j \quad (2)$$

where x_i and x_j represent the AOD data of each grid in year i and j, respectively. β denotes the direction of the variation trends from 2001 to 2021 in the study area. $\beta < 0$ indicates a downward tendency of AOD, otherwise, an increasing trend of AOD is denoted.

Mann-Kendall test is commonly carried out to measure the significance of the variation trend (Mann, 1945; Kendall, 1975). It can be calculated as follows:

$$S = \sum_{i=1}^{n-1} \sum_{j=i+1}^{n} sgn(x_j - x_i) \tag{3}$$

where $n = 21$ in this study. On the right-hand side of Equation (4),

$$sgn(x_j - x_i) = \begin{cases} 1, & x_j - x_i > 0 \\ 0, & x_j - x_i = 0 \\ -1, & x_j - x_i < 0 \end{cases} \tag{4}$$

is a sign function. The Mann-Kendall standard statistic Z can be calculated as:

$$Z = \begin{cases} \frac{S-1}{\sqrt{Var(S)}}, & S > 0 \\ 0 \quad , & S = 0 \\ \frac{S+1}{\sqrt{Var(S)}}, & S < 0 \end{cases} \tag{5}$$

where

$$Var(S) = \frac{n(n-1)(2n+5)}{18} \tag{6}$$

The absolute values of Z for the significance of the AOD variation trend are 1.65 and 1.96 at 90% and 95% confidence levels, respectively.

3.3 Hurst exponent

The Hurst exponent analysis is a statistical assessment factor to analyze the sustainability properties of variation trends (Hurst, 1951). This approach was undertaken in this study for the persistency assessment of AOD variation trends in the GBA and the detailed calculation procedure can refer to the literature (Granero et al., 2008).

The range of the Hurst exponent values is $0 < H < 1$. If $H < 0.5$, there is an anti-consistency tendency. By contrast, if $H > 0.5$, it indicates the same variation trend. The sequential data presents stochastic patterns without consistency when $H = 0.5$. The variation characteristic types were categorized in Table 1. In this way, the variation trends of AOD can be analyzed quantitatively and qualitatively based on the Hurst exponent and Theil-Sen median trend analysis.

Table 1. The trend characteristic types of AOD time series.

Indicator	Increasing ($\beta > 0$)	Decreasing ($\beta < 0$)
Sustainability ($0.5 < H < 1$)	Continuously increasing	Continuously decreasing

Non-sustainability ($0 < H < 0.5$)	First increasing then decreasing	First decreasing then increasing

4. Results and discussion

4.1 Inter-annual and monthly variations of regional mean AOD

The spatial distribution of annual mean AOD across the GBA between 2001 and 2021 is shown in Figure S1. The geographic distribution is not stable and significant spatial heterogeneity can be found in different regions. For the central regions of the study area, higher AOD were mostly concentrated, where the urban agglomeration and water bodies are located. It means that higher levels of AOD are commonly located in densely populated regions with thriving industries (He et al., 2016). Whereas lower AOD can be mainly found in the northern and eastern regions where are densely covered by vegetation. This phenomenon reveals that the AOD variations over the study region are highly related to the LULC types. Significant changes of AOD can be observed in the GBA over the study period, with an upward and then downward trend. Prominent changes in AOD can be found in the regions where construction lands and water bodies are located. It indicates anthropogenic activities and meteorological conditions have an important influence on AOD variations, which has also been suggested by other researchers (Kang et al., 2019; Ding et al., 2020).

The annual regional mean AOD values at 0.55 μm from 2001 to 2021 and the linear trend of the variations at the 95% confidence level were displayed in Figure 2. The yearly regional mean AOD is larger than 0.35 but less than 0.70 with significant oscillations. The yearly mean AOD value was peaked in 2012, thereby the study period was divided into two major periods based on the variation trend and peaked AOD, namely the pre-2012 and post-2012 periods. The year 2012 can be deemed as the turning point. During 2001-2012, interannual variations of AOD present a noticeable escalating trend of 0.0091 yr^{-1} with noticeable fluctuations. The descending trend of AOD in 2008 is more likely to be associated with the outbreak of the global financial crisis, and the values increased subsequently after the economy recovered gradually in 2009 (Buchholz et al., 2021). Nevertheless, different from the pre-2012 period, a significant steep downward trend of -0.0294 yr^{-1} was suggested from 2012 to 2021. The declining trend of AOD is more likely to be attributed to the implementation of a series of air pollution control policies enacted by the government and relevant institutes (Ma et al., 2019; Zhang et al., 2012). Thus, the overall annual mean variations over the study period show a significantly decreasing trend of 0.0086 yr^{-1}.

Besides, the AOD exhibits significant differences in monthly mean values (Figure S2a). The maximum monthly mean AOD occurs in March, with a reduction in subsequent months. Further reversal of the declining trend was observed in August and September, and the monthly average AOD in November and December is the lowest. Monthly variations have been suggested that are more associated with climatological factors (Luo et al., 2014). Consistent with the study by Luo et al. (2014), two peaks and one low monthly mean AOD can be found during March and September, ascribed to aerosol washout by the monsoon rainfalls and their evolutions. For the GBA low-latitude region, it experienced a peak monthly mean AOD of around 0.68 before the pre-summer rain in March and April, a low AOD of about 0.54 during the pre-summer rainy period in May and

higher AOD of around 0.60 after the rainfall in August and September. Evident seasonal characteristics of AOD can be observed (Figure S2b). Spring has the highest AOD reaching above 0.6, followed by summer and autumn. Winter has the lowest AOD (around 0.45). Spring was the most polluted season across the GBA over the study period, a possible reason is the high level of dust and airborne sand from natural surfaces of local and long-distance sources (i.e., South Asia, north and northwest China) (Zheng et al., 2022; Wong et al., 2013a). Additionally, frequent biomass burning activities from Southeast Asia have also been found in spring (Deng et al., 2008). It should be mentioned that high AOD is not equal to high aerosol concentration and brings serve air pollution issues, as meteorological conditions exert prominent effects on AOD. For example, higher AOD tends to accumulate in summer, perhaps because the summer heat stimulates photochemical reactions, resulting in an increase in aerosol loading (Li & Wang, 2014; Dickerson et al., 1997). Moreover, high relative humidity and high temperature in summer can enhance the oxidation of aerosol precursors (i.e., sulfur dioxide), as well as facilitate the fine-mode and other secondary pollutant particles (Yang et al., 2022). Lower AOD values can be observed in winter in the GBA region, which is more likely speculated to be mainly due to higher wind speed and dry weather conditions in winter than in summer (Chen et al., 2014; Man & Shih, 2001). As lower relative humidity can alleviate the hygroscopic growth of aerosols, and higher wind speed promotes aerosol diffusion, dilution and circulation (Yu et al., 2022). The spatial distribution of multi-year seasonal AOD over the GBA region has been displayed in Figure S3. It can be found that spring and summer have higher AOD, similar to the annual distribution, higher AOD values are commonly accumulated in urban and coastal areas. This phenomenon is more likely to ascribe to anthropogenic emissions, long-distance transport and hygroscopic growth of aerosols.

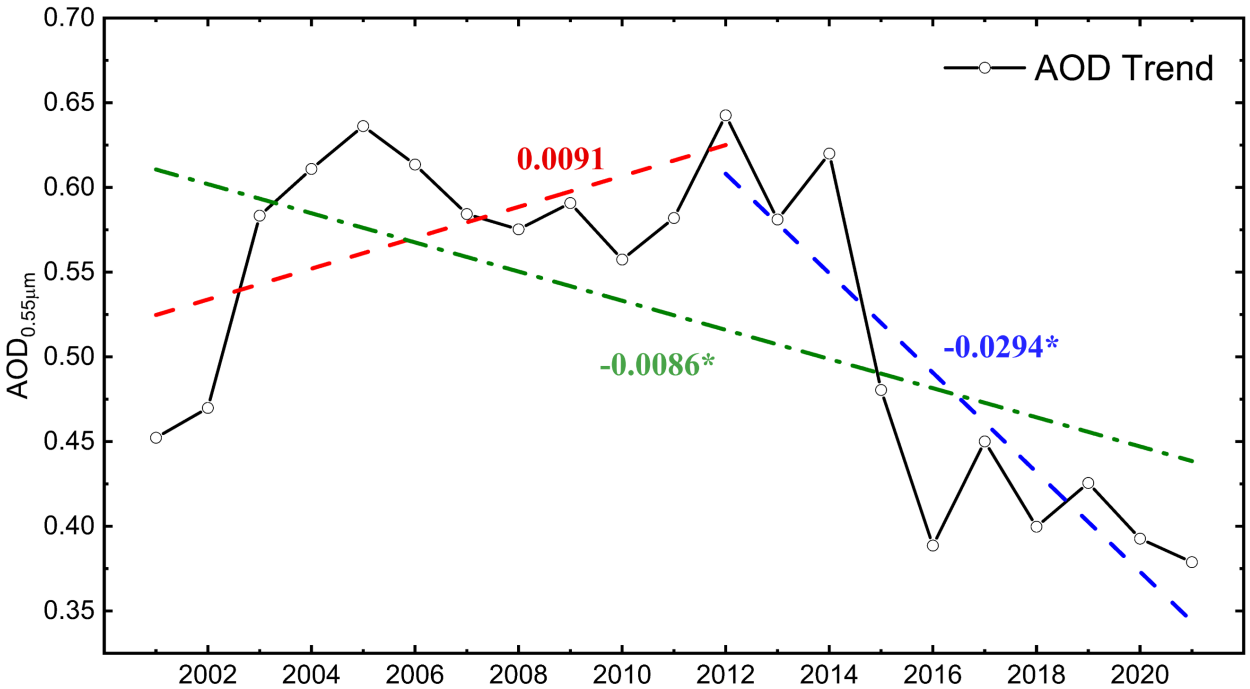

Figure 2. Inter-annual variations of regional mean AOD over the GBA with the linear trend (yr^{-1}) in three different periods, namely 2001-2012 (red), 2012-2021 (blue) and 2001-2021 (green). * represents the trends passing the 95% confidence level.

4.2 Monthly-average AOD trends in different districts based on ESMD

Figure 3 displays monthly-average AOD variation trends at the city level based on ESMD. The orange dots denote the original monthly-average AOD and blue dashed curves are the non-linear variation trends based on ESMD. From the perspective of the city-scale, two major changing trends can be categorized: increasing-fluctuating-decreasing and increasing-stable-decreasing. Increasing-stable-decreasing was mainly presented in the northern regions of the study area, like Zhaoqing, Foshan, Guangzhou and Huizhou, same as the whole GBA. AOD trends in remaining cities mainly show the increasing-fluctuating-decreasing trend. Because of the differences in meteorological conditions, geographical environment, economic development, policies and so on, AOD trends are not entirely consistent across cities (Zheng et al., 2022). Interestingly, for both increasing-stable-decreasing and increasing-fluctuating-decreasing trends, AOD increases before 2004 and presents a stable or slight fluctuation between 2004 to 2012, then a significant, continuous downward trend can be found after 2012. These findings are consistent with the annual AOD changes. The results illustrate that the year 2012 can be deemed as the turning point, with opposite trends observed before and after 2012. Moreover, different from linear regression, ESMD is an effective method to reveal AOD variations that can accurately identify non-linear and specific AOD trends.

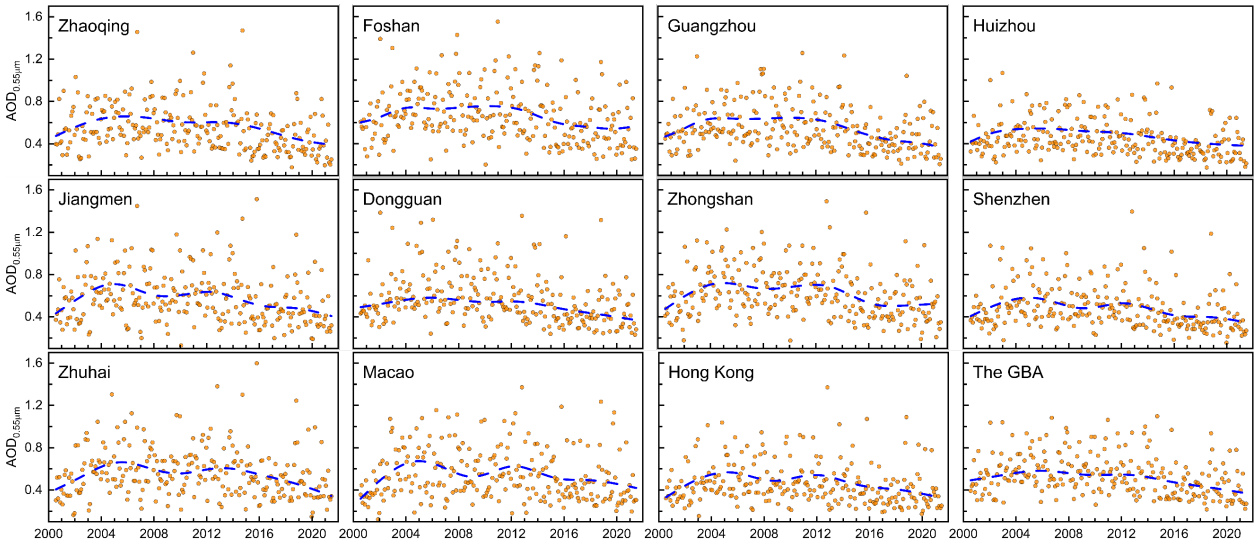

Figure 3. Monthly-average AOD trends at pixel level and city level based on ESMD. The orange dot represents the monthly-average AOD values and the blue dashed line denotes the AOD variation trend derived by ESMD.

4.3 Spatiotemporal AOD trends and the persistence of AOD dynamics

In addition to regional descriptions of AOD variation trends, a long-term variation trend analysis was carried out using the annual averaged AOD of individual pixels based on the Theil-Sen method. The Mann-Kendall test was applied in the significance test over the GBA from 2001 to 2021. The monotonic tendency can be detected from the quantitative perspective. Figure 4 displays the AOD variation trends and their significance examination. During the 21-year study period, the derived

β varies from -0.048 to 0.05 and the decreasing trend is elevated in the western areas of the GBA compared with that in the eastern. In addition, majority areas pass the 95% confidence level significance test except for some coastal regions (Figure 4d). Interestingly, the variation trends for two sub-periods present distinct distribution patterns, with an upward AOD trend in most regions of the GBA for the pre-2012 period, while a decreasing trend dominated across the study area for the post-2012 period. It is consistent with previous inter-annual trend analysis results at a coarse regional scale (Section 4.1). For the pre-2012 period, the AOD variations in most areas of the GBA are manifested by the ascending trend with a variation rate under 0.025 and prominent variation values exceeding 0.05 can be found in coastal areas (Figure 4b). However, it should be mentioned that quantities of pixels fail to pass the significance test successfully, even for the 90% confidence level (Figure 4e). Referring to Figure 2, this issue tends to be ascribed to the pronounced AOD fluctuations during 2001-2012. With regard to the post-2012 period, similar to the spatial distribution pattern of the AOD trend from 2001 to 2021, a significant declining trend can be observed across the GBA and the trend variations in the eastern areas are smaller than those in the western regions (Figure 4c). The decreasing slopes in the post-2012 period are greater than the increasing slopes in the pre-2012 period, thereby a significant declining trend in most areas of the GBA is derived for the whole study period.

Additionally, to qualitatively identify the variation tendency of AOD over the GBA, that whether AOD trends varied in opposite or same directions, the Hurst exponent test at the 95% confidence level was adopted and the results have been illustrated in Figure 5. The range of the Hurst exponent is from 0.17 to 0.87. It can be found that the H value in most areas is larger than 0.5, combining the Theil-Sen trend analysis results shown in Figure 4a, which demonstrate consistent descending trends of AOD after the study period in most regions of the GBA. Furthermore, stronger persistence (> 0.65) can be observed mainly in Zhongshan, Dongguan and the border between Shenzhen and Hong Kong SAR. Nevertheless, some regions showing slightly inconsistent variation trends ($0.3 < H < 0.5$), were mainly concentrated in Guangzhou, Huizhou and some areas in Zhaoqing. It means that the inconsistent areas tend to present an upward trend of AOD after the study period, possibly due to fluctuant meteorological conditions and the intensifying of human activities like urbanization and overgrazing (Peng et al., 2012).

In conclusion, the spatiotemporal variations and consistency of AOD over the GBA have been analyzed quantitatively and qualitatively pursuant to the Hurst exponent and Theil-Sen analysis methods. The AOD has significantly declined in favor of relevant air pollution control policies in recent years. Moreover, the descending trend tends to exhibit a consistent declining tendency for most areas in the GBA after the study period. However, the regions fail to pass the significant tests, indicating the future trend of AOD in these areas cannot be determined accurately and reliably. Consequently, specific emission regulations are supposed to be formulated and continuous concerns are indispensable in the regions with the opposite variation direction or failing to pass the significant tests.

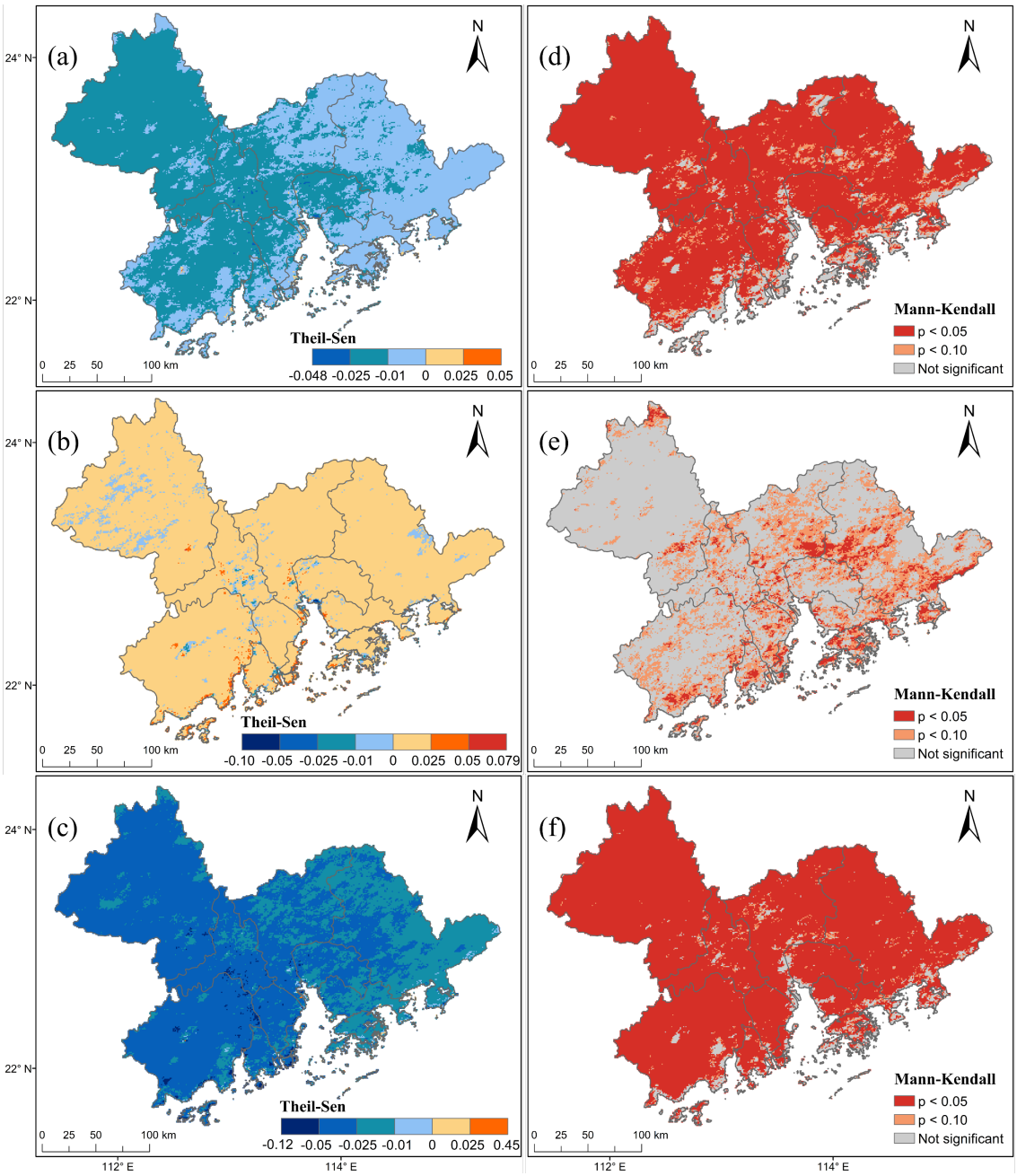

Figure 4. Spatial variations of AOD trends in the GBA from (a) 2001 to 2021; (b) 2001 to 2012; and (c) 2012 to 2021; as well as corresponding significance test results in (d) 2001-2021; (e) 2001-2012; and (f) 2012-2021.

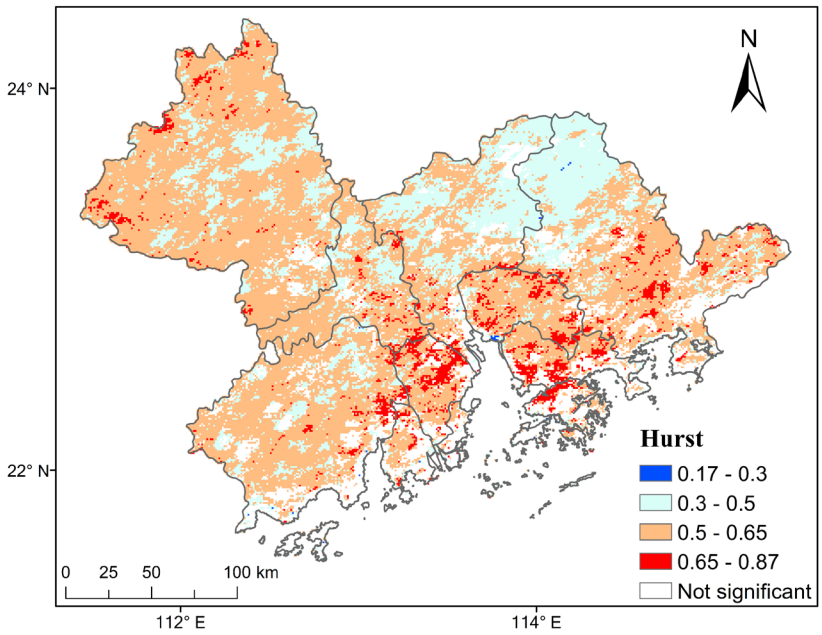

Figure 5. The persistence of AOD variation tendency over the GBA from 2001 to 2021.

4.4 AOD variations influenced by LULC and LULCC

The statistical characteristics of AOD over these six different LULC types in 2001 and 2020 have been summarized in Table 2. Discernible discrepancies in AOD values over different LULC types can be observed, with relatively high values for unused land, water bodies and construction land, while low AOD values concentrate in the regions with grassland, cropland and forests, which are also suggested by other researchers (Nair et al., 2022; Yang & Jiang, 2021). Among them, unused lands have the highest mean AOD values. It is because barren areas are generally deemed as potential dust sources, leading to elevated mean AOD (Kim et al., 2013). Water bodies have the second-largest mean AOD values with the widest range. In addition to the natural suspension of silt, the effects of human activities should be considered, such as diesel workboats plying. Moreover, major roads along the riverbanks serve heavy traffic, resulting in huge emissions (Nair et al., 2022). Relatively low AOD and clean air are in regions covered by woodlands, croplands and grasslands as vegetation is capable of absorbing atmospheric aerosol/particles and abating the ground aerosol. Different from previous studies (Liu et al., 2020), the mean AODs of grasslands are greater than those of croplands in the GBA, presumably caused by the geographical locations of the grasslands and croplands in the study area. As depicted in Figure 1b, grasslands in the study area are mostly located around urban areas or water bodies, whereas croplands are close to the forests. Thus, the AOD has been affected, showing different AOD characteristics in grasslands and croplands compared with previous studies. The discrepancies of AOD values in the LULC types can be denoted as the differentiation between anthropogenic and natural aerosols. Additionally, the AOD of these six different LULC types significantly decreased from 2001 to 2020. Unused lands have the largest decline by 23% for the mean values and the maximum values have descended from 1.12 to 0.86. AOD variations not only depend on anthropogenic emissions, but also related to meteorological parameters, climate change, geographic factors and socio-economic indices (He et al., 2016; Yu et al., 2022; Li & Wang, 2014). Additionally, AOD is

spatially autocorrelated to some extent due to the diffusion and transport of aerosol particles (Yang & Hu, 2018). Namely, AOD at a given location would be also affected by the adjacent areas. Furthermore, the standard deviations (SD) of all LULC types show a downward trend, implying the spatial differences of AOD decreased significantly and the air quality has been enhanced over the study area to some extent.

Table 2. The statistical characteristic of AOD based on different LULC types over the GBA.

LULC	2001				2020			
	Min	Max	Mean	SD	Min	Max	Mean	SD
Woodlands	0.101	0.812	0.401	0.071	0.053	0.764	0.346	0.063
Grasslands	0.128	0.844	0.448	0.082	0.087	0.798	0.379	0.078
Construction lands	0.140	0.968	0.465	0.096	0.092	0.969	0.391	0.083
Croplands	0.169	0.832	0.437	0.068	0.015	0.772	0.360	0.057
Water	0.068	1.430	0.473	0.137	0.019	1.370	0.404	0.131
Unused lands	0.174	1.12	0.599	0.124	0.152	0.862	0.459	0.078

To quantify the impacts of LULCC on the AOD changes, the decreasing rates of AOD have been calculated to compare the effects of land use pattern shift on AOD changes between 2001 and 2020 across the GBA (Figure 6). The decreasing rates of mean AOD for different LULC types were derived by using the discrepancies between the mean AOD values in 2001 and 2020 divided by the average AOD values in 2001 ($(AOD_{2020} - AOD_{2001})/AOD_{2001}$). It can be found that woodland is the main LULC type in the GBA and construction land occupies the second largest area with an increase from 7,047 km^2 to 8,511 km^2. Followed by water bodies, it remains in a relatively stable state of approximately 8%. The area of cropland has been extended significantly from roughly 2,458 km^2 to 4,024 km^2. Analogously, Grassland shows a slightly upward trend accounting for from 2.3% to 2.9%. By contrast, significant degradation of unused land can be observed. From the perspective of LULCC, other than construction land, other LULC types are significantly changed.

As discussed above, the AOD considerably decreased from 2001 to 2020 for all LULC types. Thus, there was still a downward trend of AOD in non-LULCC areas, while the decrease in these areas was irrespective of the LULCC, mainly due to meteorological changes and policy regulations and so on. To minimize uncertainties and disturbance, the decreasing rates in the non-LULCC areas were used as a reference to discuss the impacts of LULCC on AOD changes (Yang & Jiang, 2021; Nair et al., 2022). Subsequently, a statistical comparison of the AOD decreasing rates under different land use types was performed to imply the effects of LULCC. As illustrated in Figure 6a, the declining rates in conversion from woodland to other LULC types are lower than those in the regions with non-LULCC (15.91%), especially when woodland is converted to water bodies or unused land. For grassland and cropland, a similar distribution pattern of the decreasing rate can be discovered (Figure 6b and 6d), with the greatest decreasing rate existing in converting to woodland, while smaller declining rates can be found when converting to unused land and construction land. An analogous distribution pattern can be observed in the conversion of water and unused land to other LULC types (Figures 6e and 6f). There is no transformation from water or unused land into cropland. Differently, the declining rates in the conversion from water to other

types are less than those in the conversion from unused land to other types. Interestingly, there is no shift from construction land to other LULC types in the GBA during the study period, with a reducing rate of 17.42% that can be attributed primarily to emission control and other air pollution regulations (Figure 6c). The results elucidate that the drop-in rate is larger when the LULC types with higher AOD values are converted to the types with lower AOD values, while there are smaller decreasing rates when the types with lower AOD are transformed into the types with higher AOD values. The LULCC patterns can also indicate different intensities of human activities. For example, construction lands are generally deemed as high intensity owing to commercial and industrial activities, heavy traffic flow and human mobility, which are the major sources of anthropogenic aerosols. The vegetation-covered areas are less affected by human activities and indicate the natural sources of aerosols. Moreover, it has been suggested that vegetation can contribute to weakening aerosol pollution due to deposition (Yang & Jiang, 2021). When the vegetation-covered types were transformed into man-made lands, intensified human activities tend to increase AOD, leading to lower decreasing rates in these areas than in the unchanged vegetation coverage areas. In conclusion, distinct heterogeneity can be found due to LULC types and LULCC. Furthermore, the LULCC can also make contributions to the dynamics of AOD. When the unused and constructed lands are converted to natural lands, it is beneficial for alleviating the AOD values due to the lower anthropogenic emissions and dust; otherwise, higher AOD can be found. The ecological security, agricultural development and rational urbanization pattern is supposed to be formed by promoting low-efficiency land and unused land. It is recommended that vegetation coverage areas should be restrained from converting to construction land. Simultaneously, the comprehensive promotion of environment-friendly, low-carbon, healthy lifestyle and consumption is paramount.

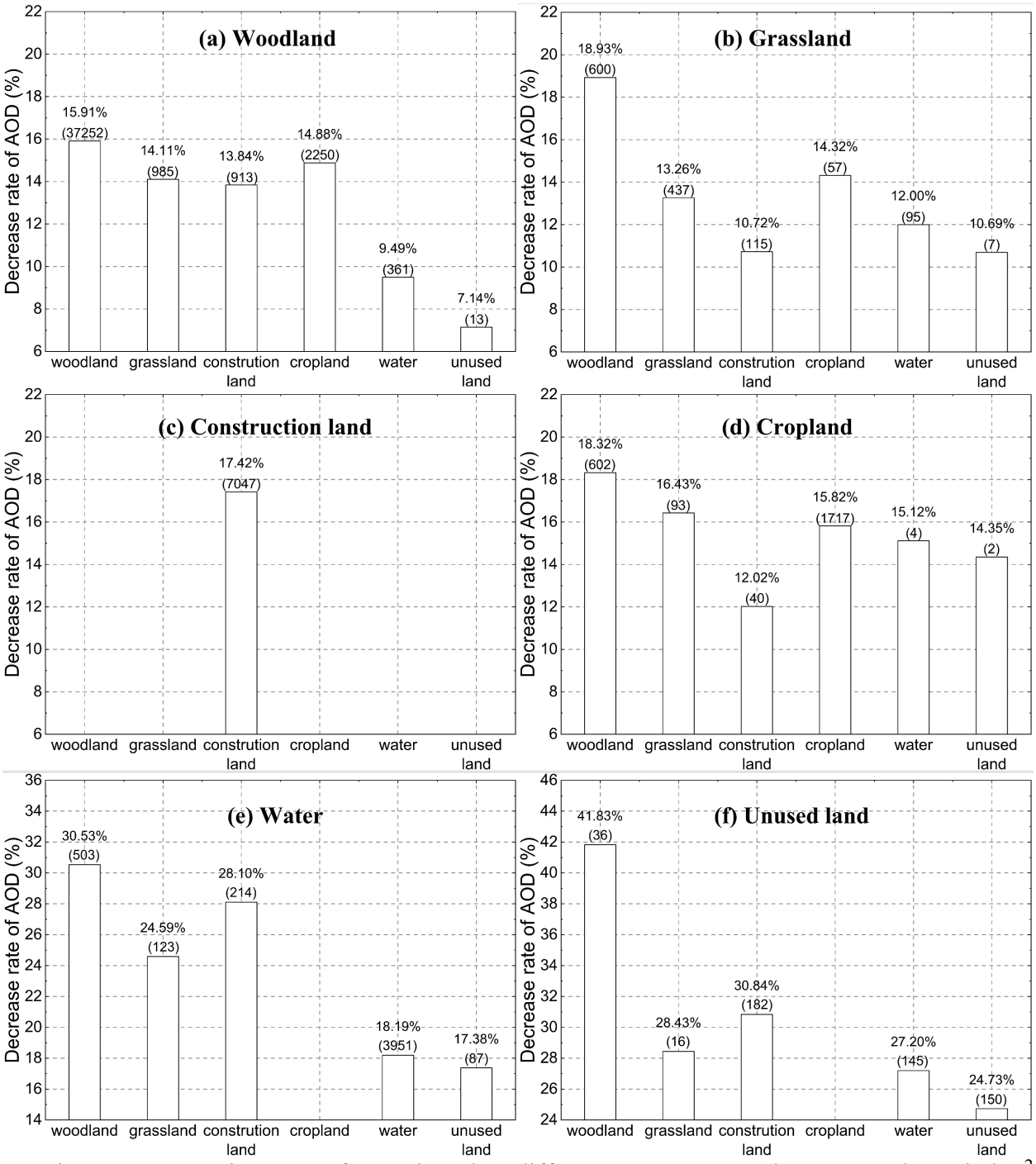

Figure 6. Decreasing rates of AOD based on different LULC types. The converted area in km^2 is in the parenthesis. The Y-axis denotes the decreasing rate of annual mean AOD of corresponding LULC types in the GBA from 2001 to 2020. The X-axis represents the LULC types in 2020, where individual bar graphs represent the LULC types in 2001, namely (a) woodland, (b) grassland, (c) construction land, (d) cropland, (e) water and (f) unused land.

5. Discussion

In our study, the AOD variation trends over two decades in the GBA region were explored from multi-spatiotemporal scales using satellite-based AOD data. Compared to previous studies, apart from the overall regional varying trend, the non-monotonic oscillations at the city level and the changing trend at the pixel level as well as its persistence were also studied. Different from linear trends, non-linear tendencies based on ESMD at the city level can provide more detailed variations. The results can advance the understanding of the AOD variations in each city and facilitate specific mitigation policies for individual cities. Additionally, the AOD variation trend and its persistence at the pixel level were evaluated quantitatively and qualitatively based on the Theil-Sen trend analysis and Hurst exponent methods, which can assist the assessment of AOD spatiotemporal evolution pattern but were rarely presented in previous studies. The results show that AOD has significantly decreased in recent years, and the decline tends to be persistent for most areas in the GBA. Finally, using the AOD changing rates of non-LULCC areas as a reference, the LULCC has been suggested that have an important impact on the AOD dynamics, as the LULCC is generally related to different intensities of human activities.

Although a relatively comprehensive AOD variations analysis over the GBA region has been performed in our study, there are still some limitations. First, due to the limitation of satellite-based AOD observations, the causes of AOD changes cannot be explored deeply from the perspective of aerosol composition. Future analysis should focus on the interactions between the aerosol compositions and meteorological conditions, which is helpful to deepen the understanding of the variations of AOD physical and optical compositions. Confined to the LULC data and analysis method, the effects of LULCC on AOD dynamics are analyzed at the regional level, with the intensities of human activities considered to be the paramount contributions. The results can provide a basic reference for regional environmental governance, whereas the responses of AOD to the LULCC might differ in different regions owing to the atmospheric circulation, climatic factors, geographical features and etc. Consequently, further investigations about the relationships between the driven factors and AOD dynamic at a finer spatiotemporal scale are desirable for a more detailed and comprehensive understanding of AOD characteristics and mechanisms.

6. Conclusion

Multi-spatiotemporal variation trends of AOD and sustainability of the tendency in the GBA from 2001 to 2021 were studied based on the ESMD, Theil-Sen median trend analysis and Hurst exponent method in this study. The Mann-Kendall test was employed for identifying the prominent trends as well. From the temporal perspective, the year 2012 was an apparent turning point in the GBA. Although the variation trend of AOD in the GBA fluctuated over the study period, with a slight increase (0.009 yr^{-1}) followed by a steep decrease (-0.03 yr^{-1}), an overall significant downward trend can be found during the 21-year period. Besides, higher AOD can be observed in spring and summer, whereas winter and autumn have lower levels of AOD. There are two major non-linear changing trends, namely the increasing-stable-decreasing trend in most northern cities and the increasing-fluctuating-decreasing trend in remaining cities. An increasing trend can be observed before 2004 and a significant decline after 2012. A stable or slightly fluctuant tendency can be found during 2004-2012. From the spatial perspective, the northern cities exhibit an increasing-stable-decreasing trend of monthly-average AOD and the increasing-fluctuating-

decreasing trend can be found in remaining cities. The decreasing rates are greater in western regions than those in eastern regions. Furthermore, majority areas present a considerable decrease with long-term persistence. Nonetheless, there should be a continuous focus on the areas with increasing or undetermined tendencies. In addition, prominent spatial heterogeneity is present over different LULC types. Specifically, unused land, water bodies and construction land have higher AOD values, whereas lower AOD values generally concentrate in the areas covered by woodland, grassland and cropland. The results imply that slow decreasing rates can be found when LULC types with low AOD values are converted to types with elevated AOD values, otherwise, high decreasing rates can be observed. In conclusion, by evaluating the long-term variation trends and periodicities of AOD, the persistence of the tendencies and the impact of LULCC on AOD change, our study provides a comprehensive and scientific basis for regional environmental protection and urban planning agencies.

References

Buchholz RR, Worden HM, Park M et al (2021) Air pollution trends measured from Terra: CO and AOD over industrial, fire-prone, and background regions. Remote Sensing of Environment 256: 112275. https://doi.org/10.1016/j.rse.2020.112275

Charlson RJ, Schwartz SE, Hales JM et al (1992). Climate forcing by anthropogenic aerosols. Science, 255(5043), 423-430. https://doi.org/10.1126/science.255.5043.423

Che H, Gui K, Xia X et al (2019). Large contribution of meteorological factors to inter-decadal changes in regional aerosol optical depth. Atmospheric Chemistry and Physics, 19(16), 10497-10523. https://doi.org/10.5194/acp-19-10497-2019

Chen J, Xin J, An J et al (2014). Observation of aerosol optical properties and particulate pollution at background station in the Pearl River Delta region. Atmospheric research, 143, 216-227. https://doi.org/10.1016/j.atmosres.2014.02.011

Deng JS, Wang K, Hong Y, Qi JG (2009) Spatio-temporal dynamics and evolution of land use change and landscape pattern in response to rapid urbanization. Landscape and urban planning 92(3-4): 187-198. https://doi.org/10.1016/j.landurbplan.2009.05.001

Deng X, Tie X, Zhou X et al (2008). Effects of Southeast Asia biomass burning on aerosols and ozone concentrations over the Pearl River Delta (PRD) region. Atmospheric Environment, 42(36), 8493-8501. https://doi.org/10.1016/j.atmosenv.2008.08.013

Dickerson RR, Kondragunta S, Stenchikov G, Civerolo KL, Doddridge BG, Holben BN (1997) The impact of aerosols on solar ultraviolet radiation and photochemical smog. science 278(5339): 827-830. https://doi.org/10.1126/science.278.5339.827

Ding S, He J, Liu D, Zhang R, Yu S (2020) The spatially heterogeneous response of aerosol properties to anthropogenic activities and meteorology changes in China during 1980–2018 based on the singular value decomposition method. Science of The Total Environment 724: 138135. https://doi.org/10.1016/j.scitotenv.2020.138135

Dinpashoh Y, Jhajharia D, Fakheri-Fard A, Singh VP, Kahya E (2011) Trends in reference crop evapotranspiration over Iran. Journal of Hydrology 399(3-4): 422-433. https://doi.org/10.1016/j.jhydrol.2011.01.021

Granero MS, Segovia JT, Pérez JG (2008) Some comments on Hurst exponent and the long memory processes on capital markets. Physica A: Statistical Mechanics and its applications 387(22): 5543-5551. https://doi.org/10.1016/j.physa.2008.05.053
He L, Wang L, Huang B et al (2020). Anthropogenic and meteorological drivers of 1980–2016 trend in aerosol optical and radiative properties over the Yangtze River Basin. Atmospheric Environment, 223, 117188. https://doi.org/10.1016/j.atmosenv.2019.117188
He Q, Gu Y, Zhang M (2019) Spatiotemporal patterns of aerosol optical depth throughout China from 2003 to 2016. Science of The Total Environment 653: 23-35. https://doi.org/10.1016/j.scitotenv.2018.10.307
He Q, Zhang M, Huang B (2016). Spatio-temporal variation and impact factors analysis of satellite-based aerosol optical depth over China from 2002 to 2015. Atmospheric Environment 129: 79–90. https://doi.org/10.1016/j.atmosenv.2016.01.002
Hurst HE (1951) Long-term storage capacity of reservoirs. Transactions of the American society of civil engineers 116(1): 770-799. https://doi.org/10.1061/TACEAT.0006518
Jiang W, Yuan L, Wang W, Cao R, Zhang Y, Shen W (2015) Spatio-temporal analysis of vegetation variation in the Yellow River Basin. Ecological Indicators 51: 117-126. https://doi.org/10.1016/j.ecolind.2014.07.031
Kang H, Zhu B, Zhu C, de Leeuw G, Hou X, Gao J (2019) Natural and anthropogenic contributions to long-term variations of SO_2, NO_2, CO, and AOD over East China. Atmospheric Research 215: 284-293. https://doi.org/10.1016/j.atmosres.2018.09.012
Kendall MG (1975) Rank Correlation Methods. Griffin, London, UK.
Kim D, Chin M, Bian H et al (2013) The effect of the dynamic surface bareness on dust source function, emission, and distribution. Journal of Geophysical Research: Atmospheres 118(2): 871-886. https://doi.org/10.1029/2012JD017907
Kim M, Kim J, Wong MS et al (2014) Improvement of aerosol optical depth retrieval over Hong Kong from a geostationary meteorological satellite using critical reflectance with background optical depth correction. Remote Sensing of Environment 142: 176-187. https://doi.org/10.1016/j.rse.2013.12.003
Li L, Wang Y (2014). What drives the aerosol distribution in Guangdong-the most developed province in Southern China?. Scientific reports 4(1): 1-8. https://doi.org/10.1038/srep05972
Li R, Ma T, Xu Q, Song X (2018) Using MAIAC AOD to verify the $PM_{2.5}$ spatial patterns of a land use regression model. Environmental Pollution 243: 501-509. https://doi.org/10.1016/j.envpol.2018.09.026
Liu J, Ding J, Li L, Li X, Zhang Z, Ran S, Ge X, Zhang J, Wang J (2020) Characteristics of aerosol optical depth over land types in central Asia. Science of The Total Environment 727: 138676. https://doi.org/10.1016/j.scitotenv.2020.138676
Liu N, Zou B, Feng H, Wang W, Tang Y, Liang Y (2019) Evaluation and comparison of multiangle implementation of the atmospheric correction algorithm, Dark Target, and Deep Blue aerosol products over China. Atmospheric Chemistry and Physics 19(12): 8243-8268. https://doi.org/10.5194/acp-19-8243-2019
Liu Y, Park RJ, Jacob DJ et al (2004) Mapping annual mean ground-level $PM_{2.5}$ concentrations using Multiangle Imaging Spectroradiometer aerosol optical thickness over the contiguous United

States. Journal of Geophysical Research: Atmospheres 109(D22). https://doi.org/10.1029/2004JD005025
Liu, J., Rühland, K. M., Chen, J., Xu, Y., Chen, S., Chen, Q., ... & Smol, J. P. (2017). Aerosol-weakened summer monsoons decrease lake fertilization on the Chinese Loess Plateau. Nature Climate Change, 7(3), 190-194. https://doi.org/10.1038/nclimate3220
Lu J, Zhang Y, Chen M et al (2021) Estimation of monthly 1 km resolution $PM_{2.5}$ concentrations using a random forest model over "2+26" cities, China. Urban Climate 35: 100734. https://doi.org/10.1016/j.uclim.2020.100734
Luo Y, Zheng X, Zhao T et al (2014). A climatology of aerosol optical depth over China from recent 10 years of MODIS remote sensing data. International Journal of Climatology, 34(3), 863-870. https://doi.org/10.1002/joc.3728
Lyapustin A, Wang Y (2018). MODIS Multi-Angle Implementation of Atmospheric Correction (MAIAC) Data User's Guide. NASA: Greenbelt, MD, USA. https://lpdaac.usgs.gov/documents/110/MCD19_User_Guide_V6.pdf. Accessed 26 July 2022
Lyapustin A, Wang Y, Laszlo I et al (2011) Multiangle implementation of atmospheric correction (MAIAC): 2. Aerosol algorithm. Journal of Geophysical Research: Atmospheres 116(D3). https://doi.org/10.1029/2010JD014985
Ma L, Xia H, Sun J et al (2018) Spatial–Temporal Variability of Hydrothermal Climate Conditions in the Yellow River Basin from 1957 to 2015. Atmosphere 9(11): 433. https://doi.org/10.3390/atmos9110433
Ma Z, Liu R, Liu Y, Bi J (2019) Effects of air pollution control policies on $PM_{2.5}$ pollution improvement in China from 2005 to 2017: A satellite-based perspective. Atmospheric Chemistry and Physics 19(10): 6861-6877. https://doi.org/10.5194/acp-19-6861-2019
Man CK, & Shih MY (2001). Identification of sources of PM_{10} aerosols in Hong Kong by wind trajectory analysis. Journal of aerosol science, 32(10), 1213-1223.
Mann HB (1945) Nonparametric tests against trend. Econometrica 13: 245–259. https://doi.org/10.2307/1907187
Martins VS, Lyapustin A, Wang Y, Giles DM, Smirnov A, Slutsker I, Korkin S (2019). Global validation of columnar water vapor derived from EOS MODIS-MAIAC algorithm against the ground-based AERONET observations. Atmospheric Research 225: 181-192. https://doi.org/10.1016/j.atmosres.2019.04.005
Munir S, Habeebullah TM, Seroji AR, Gabr SS, Mohammed AM, Morsy EA (2013) Quantifying temporal trends of atmospheric pollutants in Makkah (1997–2012). Atmospheric Environment 77: 647-655. https://doi.org/10.1016/j.atmosenv.2013.05.075
Nair M, Dey S, Bherwani H, Ghosh AK (2022) Long-term changes in aerosol loading over the 'BIHAR' State of India using nineteen years (2001–2019) of high-resolution satellite data (1×1 km^2). Atmospheric Pollution Research 13(1): 101259. https://doi.org/10.1016/j.apr.2021.101259
Peng J, Liu Z, Liu Y, Wu J, Han Y (2012) Trend analysis of vegetation dynamics in Qinghai–Tibet Plateau using Hurst Exponent. Ecological Indicators 14(1): 28–39. https://doi.org/10.1016/j.ecolind.2011.08.011
Pozzer A, De Meij A, Yoon J, Tost H, Georgoulias AK, Astitha M (2015). AOD trends during 2001–2010 from observations and model simulations. Atmospheric Chemistry and Physics 15(10): 5521-5535. https://doi.org/10.5194/acp-15-5521-2015

Qin K, Wu L, Wong MS et al (2016) Trans-boundary aerosol transport during a winter haze episode in China revealed by ground-based Lidar and CALIPSO satellite. Atmospheric environment 141: 20-29. https://doi.org/10.1016/j.atmosenv.2016.06.042

Qin Y, Li B, Chen Z, Chen Y, Lian L (2018) Spatio-temporal variations of nonlinear trends of precipitation over an arid region of northwest China according to the extreme-point symmetric mode decomposition method. International Journal of Climatology 38(5): 2239-2249. https://doi.org/10.1002/joc.5330

Ramanathan VCPJ, Crutzen PJ, Kiehl JT, Rosenfeld D (2001). Aerosols, climate, and the hydrological cycle. science, 294(5549), 2119-2124. https://doi.org/10.1126/science.1064034

Satheesh SK, Moorthy KK (2005). Radiative effects of natural aerosols: A review. Atmospheric Environment, 39(11), 2089-2110. https://doi.org/10.1016/j.atmosenv.2004.12.029

Sen PK (1968) Estimates of the regression coefficient based on Kendall's tau. Journal of the American statistical association 63(324): 1379-1389. https://doi.org/10.1080/01621459.1968.10480934

Shi Y, Lau AKH, Ng E, Ho HC, Bilal M (2021) A Multiscale Land Use Regression Approach for Estimating Intraurban Spatial Variability of $PM_{2.5}$ Concentration by Integrating Multisource Datasets. International Journal of Environmental Research and Public Health 19(1): 321. https://doi.org/10.3390/ijerph19010321

Shu Z, Liu Y, Zhao T et al. (2022). Long-term variations in aerosol optical properties, types, and radiative forcing in the Sichuan Basin, Southwest China. Science of The Total Environment, 807, 151490. https://doi.org/10.1016/j.scitotenv.2021.151490

Silva RA, West JJ, Zhang Y et al (2013). Global premature mortality due to anthropogenic outdoor air pollution and the contribution of past climate change. Environmental Research Letters, 8(3), 034005. https://doi.org/10.1088/1748-9326/8/3/034005

Sogacheva L, Rodriguez E, Kolmonen P et al (2018). Spatial and seasonal variations of aerosols over China from two decades of multi-satellite observations–Part 2: AOD time series for 1995–2017 combined from ATSR ADV and MODIS C6. 1 and AOD tendency estimations. Atmospheric Chemistry and Physics, 18(22), 16631-16652. https://doi.org/10.5194/acp-18-16631-2018

Superczynski SD, Kondragunta S, Lyapustin AI (2017) Evaluation of the multi-angle implementation of atmospheric correction (MAIAC) aerosol algorithm through intercomparison with VIIRS aerosol products and AERONET. Journal of Geophysical Research: Atmospheres 122(5): 3005-3022. https://doi.org/10.1002/2016JD025720

Tabari H, Hosseinzadeh Talaee P, Ezani A, Shifteh Some'e B (2012). Shift changes and monotonic trends in autocorrelated temperature series over Iran. Theoretical and Applied Climatology 109(1): 95-108. https://doi.org/10.1007/s00704-011-0568-8

Theil H (1950). A rank-invariant method of linear and polynomial regression analysis. Indagationes mathematicae 12(85): 173. https://doi.org/10.1007/978-94-011-2546-8_20

Tong S, Lai Q, Zhang J et al (2018) Spatiotemporal drought variability on the Mongolian Plateau from 1980–2014 based on the SPEI-PM, intensity analysis and Hurst exponent. Science of the Total Environment 615: 1557-1565. https://doi.org/10.1016/j.scitotenv.2017.09.121

Wang H, Xie SP, Kosaka Y, Liu Q, Du Y (2019) Dynamics of Asian summer monsoon response to anthropogenic aerosol forcing. Journal of Climate 32(3): 843-858. https://doi.org/10.1175/JCLI-D-18-0386.1

668 Wang JL, Li ZJ (2013) Extreme-point symmetric mode decomposition method for data analysis.
669 Advances in Adaptive Data Analysis 5(03): 1350015.
670 https://doi.org/10.1142/S1793536913500155
671 Wang X, Chen Y, Li Z, Fang G, Wang F, Liu H (2020) The impact of climate change and human
672 activities on the Aral Sea Basin over the past 50 years. Atmospheric Research 245: 105125.
673 https://doi.org/10.1016/j.atmosres.2020.105125
674 Wang X, Li T, Ikhumhen HO, Sá RM (2022) Spatio-temporal variability and persistence of $PM_{2.5}$
675 concentrations in China using trend analysis methods and Hurst exponent. Atmospheric Pollution
676 Research 13(1): 101274. https://doi.org/10.1016/j.apr.2021.101274
677 Wilcox RR (2001) Theil-Sen estimator. Fundamentals of modern statistical methods. New York:
678 Springer-Verlag, 207-210.
679 Wong MS, Lee KH, Nichol JE, Li Z (2010) Retrieval of Aerosol Optical Thickness Using MODIS
680 500×500 m^2, a Study in Hong Kong and the Pearl River Delta Region. IEEE Transactions on
681 Geoscience and Remote Sensing 48(8): 3318-3327. https://doi.org/10.1109/TGRS.2010.2045124
682 Wong MS, Nichol JE, Lee KH (2011) An operational MODIS aerosol retrieval algorithm at high
683 spatial resolution, and its application over a complex urban region. Atmospheric Research 99(3-
684 4): 579-589. https://doi.org/10.1016/j.atmosres.2010.12.015
685 Wong MS, Nichol JE, Lee KH (2013a). Estimation of aerosol sources and aerosol transport
686 pathways using AERONET clustering and backward trajectories: a case study of Hong Kong.
687 International Journal of Remote Sensing, 34(3), 938-955.
688 https://doi.org/10.1080/01431161.2012.714500
689 Wong MS, Shahzad MI, Nichol JE, Lee KH, Chan PW (2013b) Validation of MODIS, MISR,
690 OMI, and CALIPSO aerosol optical thickness using ground-based sunphotometers in Hong Kong.
691 International journal of remote sensing 34(3): 897-918.
692 https://doi.org/10.1080/01431161.2012.720739
693 Wu P, Christidis N, Stott P (2013). Anthropogenic impact on Earth's hydrological cycle. Nature
694 Climate Change, 3(9), 807-810. https://doi.org/10.1038/nclimate1932
695 Xiao Q, Wang Y, Chang HH, Meng X, Geng G, Lyapustin A, Liu Y (2017) Full-coverage high-
696 resolution daily $PM_{2.5}$ estimation using MAIAC AOD in the Yangtze River Delta of China.
697 Remote Sensing of Environment 199: 437-446. https://doi.org/10.1016/j.rse.2017.07.023
698 Yang J, Hu M (2018). Filling the missing data gaps of daily MODIS AOD using spatiotemporal
699 interpolation. Science of the Total Environment, 633, 677-683.
700 https://doi.org/10.1016/j.scitotenv.2018.03.202
701 Yang N, Shi H, Tang H, Yang X 2022. Geographical and temporal encoding for improving the
702 estimation of $PM_{2.5}$ concentrations in China using end-to-end gradient boosting. Remote Sensing
703 of Environment, 269, 112828. https://doi.org/10.1016/j.rse.2021.112828
704 Yang W, Jiang X (2021) Evaluating the influence of land use and land cover change on fine
705 particulate matter. Scientific Reports 11(1): 17612. https://doi.org/10.1038/s41598-021-97088-8
706 Yin S (2021) Decadal trends of MERRA-estimated $PM_{2.5}$ concentrations in East Asia and potential
707 exposure from 1990 to 2019. Atmospheric Environment 264: 118690.
708 https://doi.org/10.1016/j.atmosenv.2021.118690

Yu X, Nichol J, Lee KH, Li J, Wong MS (2022). Analysis of Long-Term Aerosol Optical Properties Combining AERONET Sunphotometer and Satellite-Based Observations in Hong Kong. Remote Sensing, 14(20), 5220. https://doi.org/10.3390/rs14205220
Zhang Q, He K, Huo H (2012) Cleaning China's air. Nature 484(7393): 161-162. https://doi.org/10.1038/484161a
Zhang ZY, Wong MS, Nichol JE (2016) Global trends of aerosol optical thickness using the ensemble empirical mode decomposition method. International Journal of Climatology 36(13): 4358-4372. https://doi.org/10.1002/joc.4637
Zhao B, Jiang JH, Gu Y et al (2017). Decadal-scale trends in regional aerosol particle properties and their linkage to emission changes. Environmental Research Letters, 12(5), 054021. https://doi.org/10.1088/1748-9326/aa6cb2
Zheng Y, Wang X, Zhang X, Hu G (2022) Multi-spatiotemporal patterns of aerosol optical depth and influencing factors during 2000–2020 from two spatial perspectives: The entire Yellow River Basin region and its urban agglomerations. International Journal of Applied Earth Observation and Geoinformation 106: 102643. https://doi.org/10.1016/j.jag.2021.102643

Funding

This work was supported by the Research Institute for Land and Space (Grant No. 1-CD81), The Hong Kong Polytechnic University; and General Research Fund (Grant No. 15603920 and 15602619), and Collaborative Research Fund (Grant No. C7064-18GF, C4023-20GF), from the Hong Kong Research Grants Council, Hong Kong, China.

Ethics declarations

Ethical Approval

Not applicable.

Consent to Participate

Not applicable.

Consent to Publish

Not applicable.

Competing Interests

The authors declare that they have no competing interests.

Author Contributions

All authors contributed to the study conception and design. Material preparation, data collection and analysis were performed by Xinyu Yu and Man Sing Wong. The first draft of the manuscript was written by Xinyu Yu. Manuscript reviewing and editing were performed by Man Sing Wong

and Chun-Ho Liu. All authors commented on previous versions of the manuscript. All authors read and approved the final manuscript.

Availability of data and materials

All datasets used in this study are available to download by the web links given in the article.